(article starts on next page)

Research Articles

Multiple Roles of Alkanethiolate-Ligands in Direct Formation of H₂O₂ over Pd Nanoparticles

Lin Chen,* Pedro Moura, J. Will Medlin, and Henrik Grönbeck*

Abstract: Coadsorbed organic species including thiolates can promote direct synthesis of hydrogen peroxide from H₂ and O₂ over Pd particles. Here, density functional theory based kinetic modeling, augmented with activity measurements and vibrational spectroscopy are used to provide atomistic understanding of direct H₂O₂ formation over alkylthiolate(RS) Pd. We find that the RS species are oxidized during reaction conditions yielding RSO₂ as the effective ligand. The RSO₂ ligand shows superior ability for proton transfer to the intermediate surface species OOH, which accelerates the formation of H₂O₂. The ligands promote the selectivity also by blocking sites for unselective water formation and by modifying the electronic structure of Pd. The work rationalizes observations of enhanced selectivity of direct H₂O₂ formation over ligand-funtionalized Pd nanoparticles and shows that engineering of organic surface modifiers can be used to promote desired hydrogen transfer routes.

Introduction

Hydrogen peroxide, H₂O₂, is used as a mild oxidizing agent in a wide range of applications including waste water purification, bleaching and within the healthcare sector.[1] The demand for hydrogen peroxide has grown significantly worldwide owing to its use as disinfectant during the recent COVID-19 pandemic.[2] Oxidation using hydrogen peroxide is an environmentally friendly process as the only by-products are H₂O and O₂,[3] which is a clear advantage with

respect to nitric acid or chlorinated oxidizers. The production of H₂O₂ depends presently on the anthraquinone process, which requires large-scale facilities.[4] The anthraquinone process is an energy-intensive batch method that involves sequential hydrogenation and oxidation steps.[4] Direct synthesis of H₂O₂ from H₂ and O₂ over transition metals at low temperatures (275–315 K) has recently attracted growing attention as an appealing alternative production route thanks to its simplicity and low environmental impact.[5] Moreover, direct synthesis can be operated at a small-scale where H₂O₂ is produced close to the location of usage.[6,7]

Palladium catalysts have shown promising activity and selectivity towards the production of H₂O₂ and, generally, a better performance than other transition metal catalysts, such as Pt[8] and Au.[9] However, the selectivity reported to date over supported Pd nanoparticles is low, ranging from 0% to 42%.[1,10,11] The selectivity for Pd-based catalysts appears to depend on several factors, such as reactant pressures, particle size, support composition, acidity of solvents (e.g. water or ethanol containing HCl or H₂SO₄) and promoters (e.g. the presence of halides).[1,7,12–14]

The low selectivity over Pd arises from irreversible O–O bond rupture of adsorbed intermediates (O₂ and OOH) and the subsequent unselective hydrogenation to H₂O.[15] As the unwanted O–O bond breaking results in adsorbed O species, destabilizing the O-intermediate relative to O₂ and OOH may improve the selectivity.[5] An alternative possibility to enhance the selectivity is to restrict the available adsorption sites. Adsorbed O generally occupies hollow sites, whereas OOH usually binds in atop or bridge configurations.[15] Thus, selective elimination of hollow sites could prevent O–O scission.

There are mainly three strategies to eliminate the hollow sites for adsorption on Pd catalysts. The first strategy is alloying Pd with other transition metals, such as Au,[1,16,17] Ni,[18] and Sn.[19] The function of the additional metal is to isolate the active Pd-sites forming single-atom sites and electronically modify the Pd-metal.[5,20] The second strategy is to operate the reaction at high H₂ partial pressures, which effectively blocks hollow sites and thereby hinders O–O bond scission and promotes the desorption of the products.[7,12,15,21] The third strategy is to tune the three-dimensional environment of the active site via surface-bound ligands.[10,14] Although it is clear that the ligands, for example thiols, block sites on the Pd-surface, the underlying mechanism of the improved selectivity for H₂O₂ formation over ligand-decorated Pd nanoparticle is largely unknown. Lari et al.[10] measured a high selectivity (up to 80%) for

[*] L. Chen, H. Grönbeck
Department of Physics and Competence Centre for Catalysis,
Chalmers University of Technology
41296 Göteborg (Sweden)
E-mail: clin@chalmers.se
ghj@chalmers.se

P. Moura, J. W. Medlin
Department of Chemical and Biological Engineering, University of
Colorado Boulder
Boulder, CO 80303 (USA)

direct synthesis of H_2O_2 on HHDMA ligand-decorated Pd nanoparticle and rationalized the high selectivity as an effect of an electrostatic interaction between intermediates and the HHDMA ligand, which prevents the O–O bond breaking by steering the adsorption geometries of the intermediates. Related to kinetic effects of ligands is the influence of the solvent. The importance of the solvent for direct H_2O_2 formation has recently been stressed by Adams et al.[22] Direct formation of H_2O_2 over Pd nanoparticles in aqueous methanol was investigated and it was demonstrated that hydroxymethyl, which was produced from methanol in the solvent may participate in the reaction as a redox mediator to transfer both protons and electrons to the intermediates. Refs. [10,22] suggest that surface-bound species play possible roles beyond site blocking.

Herein, the reaction mechanism for direct formation of H_2O_2 from H_2 and O_2 over alkylthiolate(RS)-decorated Pd catalysts is studied by combining density functional theory calculations and first-principles based mean-field kinetic modeling using methylthiolate-modified PdH(335) and a Pd_{55} cuboctahedron hydride as model systems. Thiolates are chosen as RS self-assemble into relatively well-defined monolayers on Pd.[23] Surprisingly, the results demonstrate that the effect of the ligands extends beyond simple site blocking to direct promotion of key elementary reaction steps. An analysis of the catalyst state under reaction conditions by both computational and experimental techniques shows that the thiolates are oxidized to RSO_2, which constitutes the effective ligand. The ligands block sites and reduce the O–Pd bond strength, which hinders O–O bond rupture. Furthermore, the RSO_2 ligands mediate proton transfer from the Pd-surface to the intermediate oxygen-containing species, which accelerates the formation of H_2O_2. The simulated high selectivity is consistent with our new measurements showing a higher selectivity of ethanethiolate-coated Pd nanoparticles as compared to the uncoated case. Thus, our study uncovers multiple roles of RS-ligands in the direct formation of H_2O_2 over Pd catalysts and explains how ligands can simultaneously act as catalyst poisons (for O_2 and OOH dissociation) and promoters (for proton transfer), where the promoting RSO_2 moiety is generated in situ during reaction conditions.

Results

$Pd(335)$ and Pd_{55} in a cuboctahedral structure are chosen as model systems for direct H_2O_2 formation over Pd nanoparticles, Figure 1. A high index surface is used to model large-size nanoparticles instead of Pd(111), as surface steps are required to adsorb O_2 over Pd at high hydrogen pressures and low temperatures.[15,24] Pd(335) has micro terraces large enough between the repeated steps to model both edge and terrace sites. The Pd(335) system is treated in a four-layer (2×1) cell. The Pd_{55} cuboctahedron nanocluster is used to model a small Pd nanoparticle. The diameter of Pd_{55} is about 1.1 nm, whereas the average Pd nanoparticle diameter experimentally is about 1.3 nm.[14] Both systems are treated in the β-hydride phase, which is the thermody-
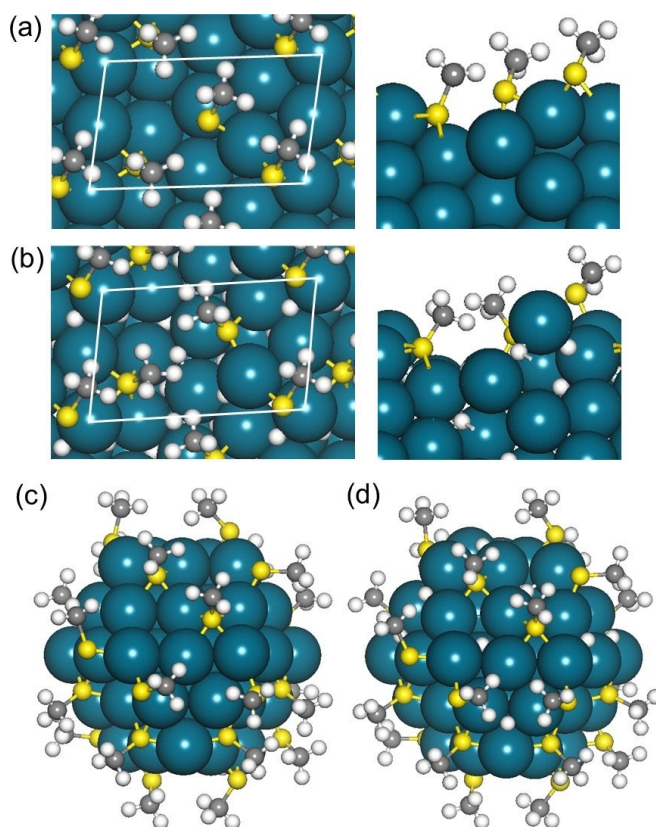

Figure 1. Considered Pd-systems. a) methylthiolate-decorated Pd(335); b) methylthiolate- decorated PdH(335). The left figures are top-views and the right figures are side-views. Pd(335) is coated with three CH_3S-ligands in the surface cell yielding a coverage of 0.38. c) methylthiolate-decorated Pd_{55} cuboctahedron; d) methylthiolate-decorated Pd_{55} in hydride phase. The nanoparticle is coated with 25 ligands, which corresponds to a coverage of 0.6. Atom color codes: Pd (blue), S (yellow), C (grey) and H (white).

namically preferred state during reaction conditions.[15] As reported previously,[25] the unmodified Pd/Al_2O_3 catalyst has a Pd dispersion close to 30 % and a mean particle size of approximately 4 nm. Despite this relatively large particle size, prior work on SAM-coated catalysts has shown that activity for certain reactions can be dominated by edge sites.[25] For example, whereas alkanethiols strongly block Pd terraces and limit furfuryl alcohol decarbonylation, alkanethiols have been shown to allow for activity over step and edge sites.[26]

The state of the catalyst during the reaction conditions

We conducted thermodynamic analyses to determine i) the coverage of the thiolates; ii) the state of Pd (metal or hydride) and iii) the stability of the thiolates under typical reaction conditions. The adsorption energy of one RS ligand in the surface cell of Pd(335) is −2.07 eV. The differential adsorption energy drops dramatically after a coverage of 0.38 (three RS in the surface cell), which is closed to the experimentally observed 1/3 monolayer coverage of C_6SH

Angew. Chem. Int. Ed. **2022**, *61*, e202213113 (2 of 9)

© 2022 The Authors. Angewandte Chemie International Edition published by Wiley-VCH GmbH

on Pd nanoparticles.[14,27] The Pd_{55} cuboctahedron has six (100) facets and eight (111) facets. The adsorption energy of one RS ligand at the (100) and the (111) facet is calculated to be −2.11 eV and −1.66 eV, respectively. Thus, the RS-ligands are preferably bound to the (100) facets at low coverage. The sequential adsorption energies of RS-ligands with increasing coverages over Pd_{55} have been calculated and the corresponding structures are shown in Figure S1 in the Supporting Information. The (111) facets start to be populated at coverages above 0.3. The differential adsorption energy drops after a coverage of 0.6 as atop sites are populated. Previous experimental studies have shown that n-alkanethiolate monolayers form $\sqrt{3}x\sqrt{3}$ R30 overlayers on Pd(111) terraces; higher coverages are expected on small nanoparticles.[27] Submonolayer coverages of sulfides are also known to coexist with alkanethiolates on Pd nanoparticle surfaces, increasing the total sulfur coverage.[27] To establish the relevant coverage during reaction conditions, we perform a thermodynamic analysis (see Figure S2). We find that the relevant coverage for Pd_{55} is 0.6 in a wide temperature range. In an experimental study,[28] a hexane-thiolate-coated Pd nanoparticle (919 atoms) was prepared at ∼40 °C and the RS-coverage was estimated to be about 0.5. Our predicted coverage of RS-coated Pd_{55} is in fair agreement with the experimental coverage, especially given that the saturation thiolate coverage is expected to decrease with increasing particle size.

The Pd catalysts have shown to be in a hydride phase during the typical reaction conditions.[15] Thus, to describe the reaction over RS-decorated Pd at low temperatures and high H_2 pressures, a hydride phase is considered. The surface sites are occupied at once when Pd is exposed to H_2 and bulk sites are eventually occupied until a total coverage of ≈0.7 is reached (β-phase).[15] To avoid the configurational complexity, we modeled the hydride phase with a coverage of 1. Thus, each octahedron in the surface slab or core of the Pd_{55} is occupied with one hydrogen atom. In addition, each hollow fcc site on the surface is occupied by hydrogen. The RS-decorated Pd(335) model contains 27 H atoms and RS-decorated Pd_{55} contains 32 H atoms. The average adsorption energy for hydrogen is −0.46 (−0.39) eV for RS-decorated Pd(335) (Pd_{55}). The average adsorption energy for H is −0.56 and −0.97 eV for non-decorated PdH(335) and $Pd_{55}H_{62}$ with one monolayer of hydrogen, respectively.

The stability of the adsorbed thiolates in an oxygen environment should be investigated as oxidation of Pd-, Ag- and Cu-bound thiolates to RSO_2 and RSO_3 has been observed in ambient conditions.[27,29] As the direct formation of H_2O_2 proceeds at (sub)ambient temperature,[14] the oxidation of the RS-ligands over Pd catalysts should be considered.

The potential energy landscape for the oxidation of thiolates on Pd(335) is shown in Figure 2(a). O_2 adsorbs with an adsorption energy of −0.47 eV at the bridge site on the edge. The thiolates strongly decrease the adsorption energy of O_2 as the adsorption energy on the bare Pd(335) surface is −1.38 eV. O_2 dissociates with a low barrier of 0.25 eV forming RS*O and adsorbed oxygen (O*). This step is exothermic by −1.16 eV. Dissociation of O_2 to 2O* is

associated with a high barrier of 1.44 eV. Thus, the oxidation of the RS-ligand is clearly favored as compared to the formation of 2O*. Further oxidation of RS*O to $RS*O_2$ has a low barrier of 0.29 eV. $RS*O_2$ desorption is prevented by a strong adsorption energy of −2.22 eV. The adsorption of an additional O_2 close to $RS*O_2$ is exothermic by −0.15 eV and the subsequent oxidation of $RS*O_2$ to $RS*O_3$(surfonate) proceeds with a barrier of 0.43 eV. The formation of $RS*O_3$ is strongly exothermic (−2.00 eV).

To investigate the potential energy surface also in the presence of hydrogen, we studied O_2 adsorption over ligand-coated PdH(335) [Figure 2(b)]. O_2 adsorbs at the edge with an adsorption energy of −0.29 eV, which shows that the hydride phase further weakens the interaction between O_2 and Pd. The adsorbed O_2 can either pick up one proton from the surface forming an O*OH species with a barrier of 0.31 eV or oxidize the RS-ligand, which is associated with a barrier of 0.53 eV. The oxidation of RS* to RS*O is thermodynamically favorable compared to O*OH formation by 0.62 eV. Further hydrogenation of O*OH to H_2O_2 is associated with a barrier of 0.67 eV, whereas oxidation of RS*O to $RS*O_2$ has a barrier of 0.54 eV. The formation of $RS*O_2$ is energetically preferred with respect to formation of H_2O_2 by 1.91 eV. The oxidation of $RS*O_2$ to $RS*O_3$ is energetically preferred (−1.65 eV) and proceeds via a barrier of 0.75 eV. We also calculated the reaction path for thiolate oxidation over the hydrogenated Pd_{55} particle (see Figure S3). $RS*O_2$ formation is also in this case strongly preferred. Importantly, the moderate barriers for the RS-oxidation indicate that RS will be converted to RSO_2 or RSO_3 during reaction conditions or during storage of the thiolate-protected Pd catalysts under ambient conditions.

To analyze the equilibrium state of the catalyst during reaction conditions, we built a reaction network for the oxidation reaction and analyzed the equilibrium coverages over Pd(335) and PdH(335) at relevant temperatures (275 to 315 K). The analysis (Figure S4) shows that thiolates are oxidized to sulfonates (RSO_3) over Pd(335), which is in agreement with experimental observations.[27] However, we find that $RS*O_2$ is the preferred species in the presence of H_2 over PdH(335). Thus, $RS*O_2$ should be considered as the effective ligand for direct H_2O_2 formation over thiolate-coated Pd nanoparticles. The reason for the difference between Pd(335) and PdH(335) is the higher barrier of the oxidation of RSO_2 to RSO_3 in the hydride case.

To experimentally verify that low-temperature exposure to O_2 and H_2 leads to formation of oxidized RSO_x groups, diffuse reflectance infrared Fourier transform spectroscopy (DRIFTS) is performed on n-hexanethiol-coated Pd/Al_2O_3 (experimental details in Supporting Information). Under O_2 flow we observe the appearance of distinct features in the spectral range between 1000 and 1200 cm^{-1} (see Figure 3-(a)). The wavenumbers are consistent with IR assignments to sulfinates and sulfonates.[29] DRIFT spectra in the C–H region (Figure 3(b)) show a significant decrease in intensity for both methylene (v_a: 2923 cm^{-1} and v_s: 2854 cm^{-1}) and methyl (v_a: 2962 cm^{-1} and v_s: 2878 cm^{-1}) stretches, possibly indicating some desorption of thiol-derived species. Following a subsequent H_2 exposure, we observe the formation of
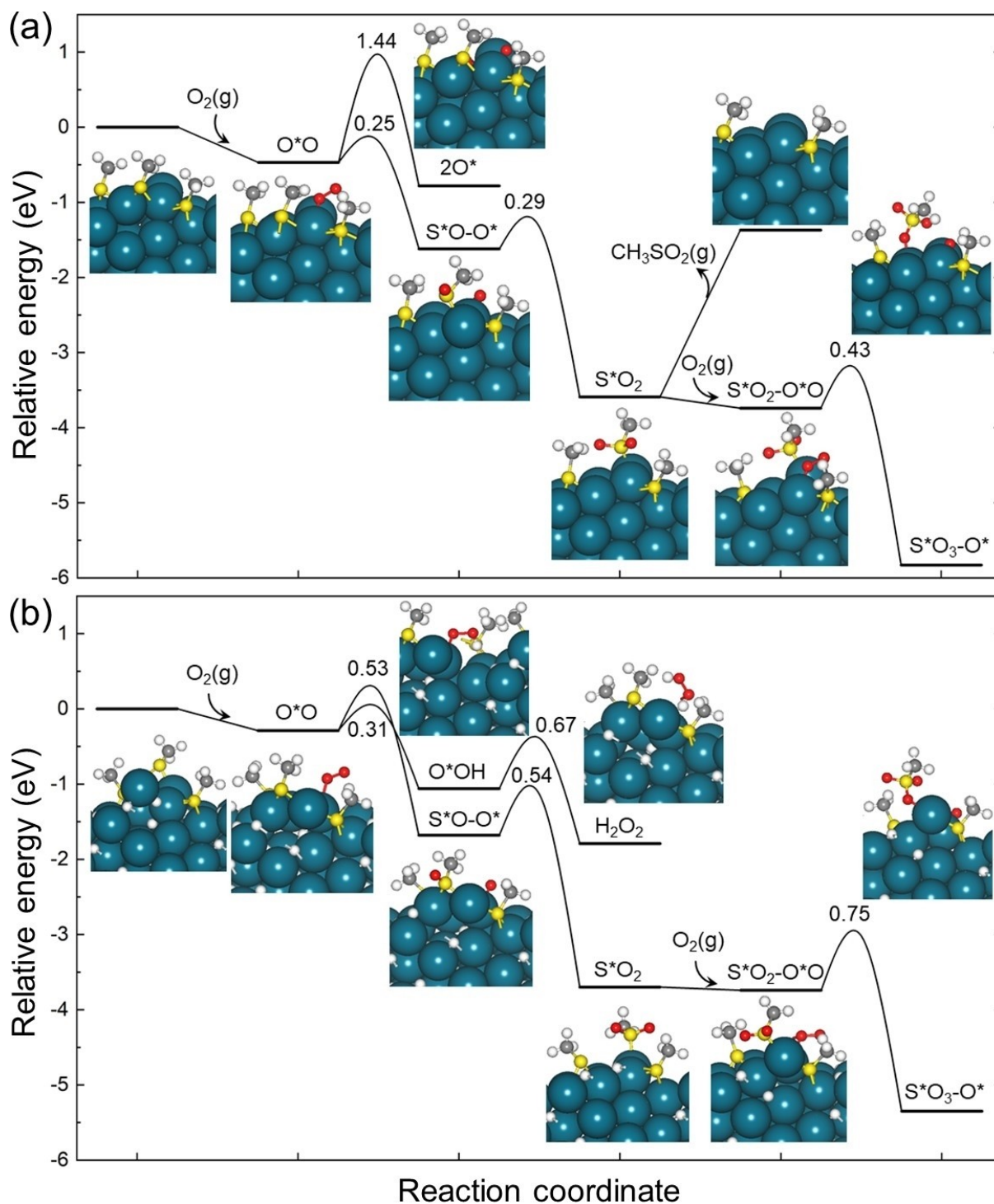
Figure 2. Potential energy landscape for the oxidation of thiolates over Pd(335) (a) and PdH(335) (b). All energies are zero-point corrected. Atom color codes: Pd (blue), S (yellow), O (red), C (grey) and H (white).

a new peak at 1238 cm^{-1}, attributed to an O–H bend, and an increase in intensity for the remaining features (Figure 3(a)). The significant intensity of peaks in the RSO$_x$ stretching region suggests that oxidized species are retained at reducing conditions, consistent with the high barriers for reduction of RSO$_2$ shown in Figure 2. Both the calculations and experi- ments indicate that long-term stability of the

thiol ligands over Pd may be an issue, as RSO$_3$ formed by deep oxidation may desorb into the solution. Controlling the selectivity via the decorated ligands may thus require continuous replenishment via the feeding of dilute levels of the ligand.[30]

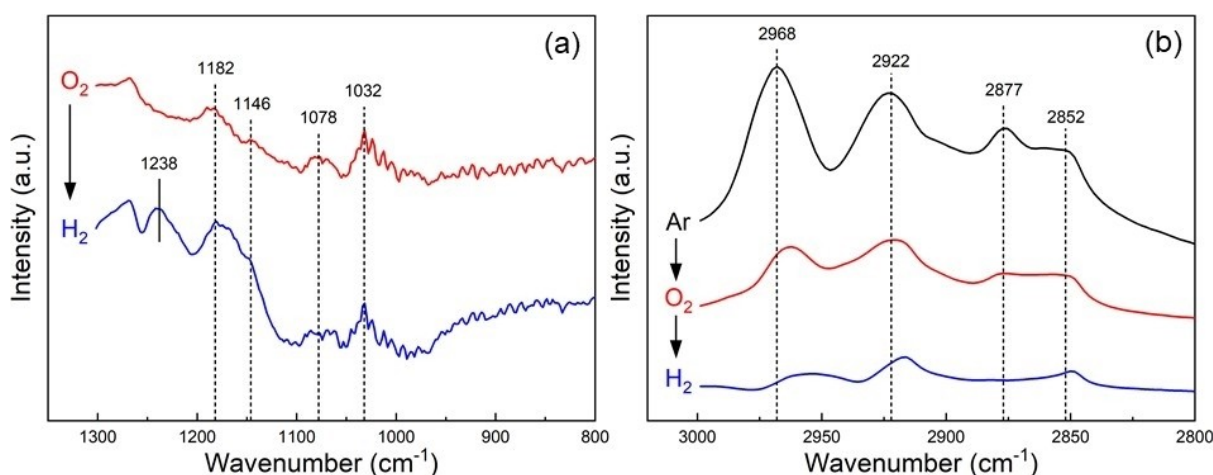Our analysis of the system during reaction conditions for direct formation over the RS-decorated Pd nanoparticle

Figure 3. DRIFT Spectra of hexanethiolated Pd on Al_2O_3 at room temperature (298 K). After argon purge (black); O_2 flow for 9 h following initial purge (red); H_2 flow for 9 h following oxidation (blue); pointing arrows indicate the order of exposure for gas flows throughout the experiment. a) S–O Region: Potential candidates for S–O stretches are highlighted with reference dotted lines; peak formed after H_2 exposure is indicated with a solid line. b) C–H Region: Features associated with C–H stretches are highlighted with dotted reference lines. Note that figure (a) reports both spectra using the pre-oxidized infrared spectrum as a background to make changes due to surface oxidation more apparent, whereas figure (b) reports spectra relative to a background collected for an uncoated catalyst to illustrate relative intensities for C–H stretching.

shows that: i) the coverage of thiolates is 0.38 over Pd(335) and 0.6 over Pd_{55}; ii) palladium is in a hydride phase and iii) thiolates are oxidized to $RS*O_x$ with $RS*O_2$ being the favorable state under direct H_2O_2 synthesis conditions.

Direct formation of H_2O_2 over RS-decorated Pd(335) and Pd_{55}

The hydrogen transfer and O–O scission steps during direct synthesis of H_2O_2 over hydrogenated, RS-decorated Pd(335) and Pd_{55} are shown in Figure 4. We focus on these steps as they determine the selectivity of the reaction. The entire potential energy landscapes are shown in Figure S5 and the relative energies for each step are listed in Table S2. For simplicity, only the thiolates close to the site for O_2 adsorption are considered to be in the oxidized state.

At the thiolate-decorated stepped PdH(335), the hydrogenation of O*O to O*OH has a barrier of 0.22 eV (Figure 4(a)). The decomposition of O*O is endothermic and associated with a high barrier of 1.68 eV. The further hydrogenation of O*OH to HO*OH is energetically favorable. There are two possibilities for the second hydrogen-transfer step. The surface-mediated route when a hydrogen atom is picked up from the surface has a barrier of 0.71 eV. An alternative possibility is to transfer the proton via the $RS*O_2$ ligand. In this ligand-mediated process, the $RS*O_2$ ligand picks up the surface hydrogen atom in an exothermic step with a barrier of 0.41 eV forming $RS*O_2H$ (a detailed structure is shown in Figure S6). The formation of such $RS*O_xH$ complexes is consistent with the observed effect of hydrogen in the DRIFTS experiments (see Figure 3(a)). Once $RS*O_2H$ has formed, the subsequent transfer to O*OH forming HO*OH proceeds spontaneously. Thus, the barrier for HO*OH formation via the ligand-mediated route is only 0.41 eV. The decomposition of O*OH species to

O*H and O* is hindered by a high barrier of 1.62 eV. The unselective hydrogenation of O*OH species to H_2O and O* proceeds via a barrier of 0.68 eV.

Due to the heavy computations connected to calculations of barriers over the palladium nanoparticles, only the critical steps of O*O dissociation (step $S*O_2$–O*O to $S*O_2$–2O*), O*OH dissociation (step $S*O_2$–O*OH to $S*O_2$–O*H–O*) and the hydrogenation of O*OH and HO*OH (pink lines) are considered explicitly for Pd_{55} (Figure 4(b) and Figure S5). One difference with respect to PdH(335) is the dissociation of RSO_2–O*O to $RS*O_2$–2O*. The dissociation of O*O to 2O* on the stepped surface is endothermic by 0.13 eV, whereas it is exothermic by 1.11 eV over the nanoparticle. The large difference could be explained by the structural flexibility of the nanoparticle. As O* prefers to locate at the hollow site, it is connected to larger local structural distortions on the stepped surface than on the nanoparticle. In addition, the coverage of the O_2 on the nanoparticle is lower than on the stepped surface. The exothermicity of O_2 dissociation over Pd_{55} gives rise to a lowering of the dissociation barrier to 0.72 eV. The decomposition barrier for O*OH to O*H and O* over the nanoparticle is calculated to be 0.40 eV, which is considerably lower than the barrier over the stepped surface. The ligand-mediated hydrogen transfer is found to be barrierless also over the nanoparticle. The barriers for O*OH hydrogenation are calculated to be 0.51 eV.

Besides the investigation on the reaction energy landscapes, we find that the effective $RS*O_2$-ligands enable a strong hydrogen bond between O*OH and $RS*O_2$, which stabilizes O*OH and hinders the reverse reaction to O*O and H*. We estimate the stabilization to be ≈0.4 eV (see Figure S8). The ligands have in this sense a similar role as regular solvents, e.g. methanol or water.
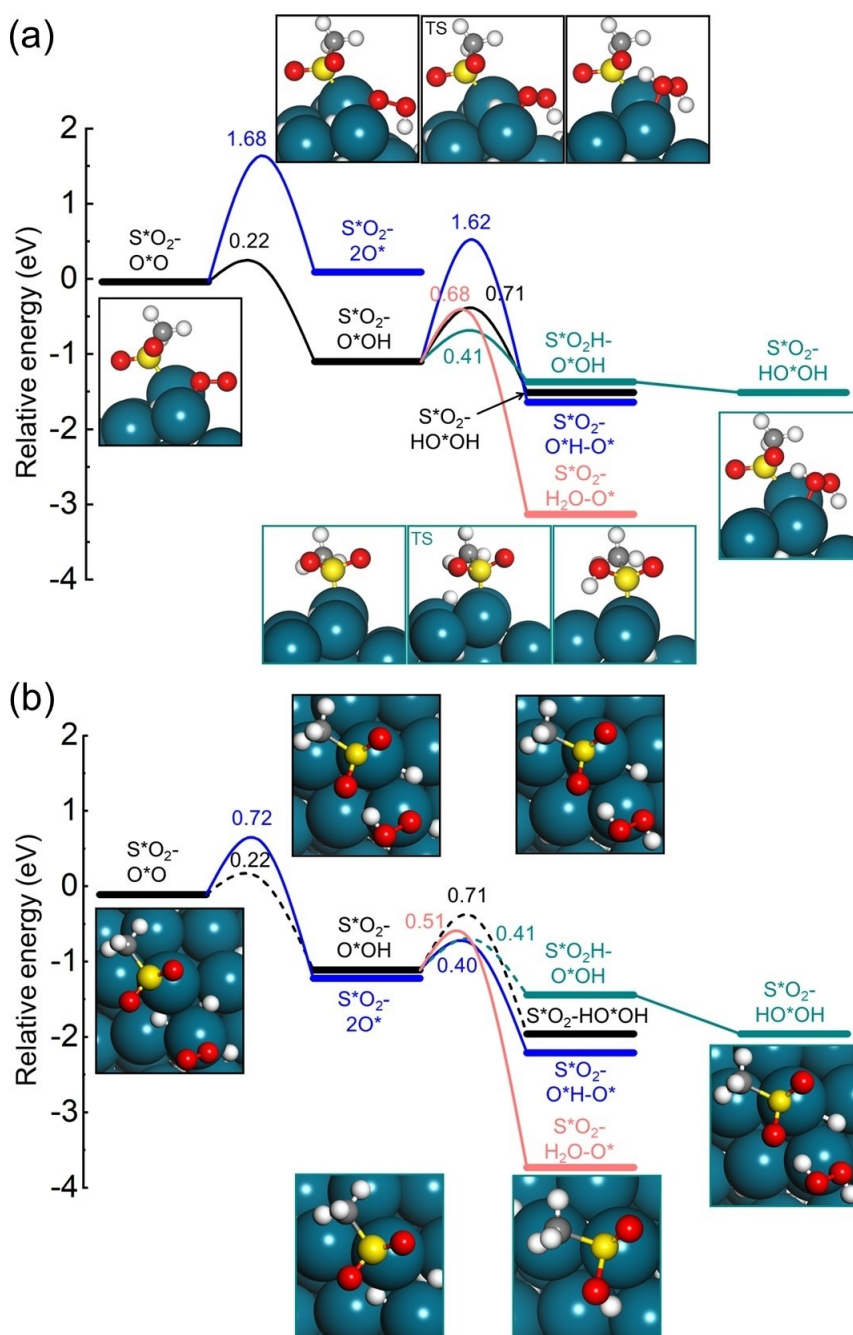
Figure 4. Potential energy landscape for direct H_2O_2 formation from H_2 and O_2 over RS- decorated PdH(335) and Pd_{55} cuboctahedron in hydride phase. The direct H_2O_2 formation path with proton transfer via the surface Pd is plotted with black lines, the direct H_2O_2 formation path with proton transfer via the ligand RSO_2 is plotted with gree lines, the H_2O formation path from O—O bond breaking is plotted with blue lines and the H_2O formation path from hydrogenation over OOH and H_2O_2 is plotted with red lines. The reaction barriers over the small nanoparticle with dashed lines are taken from the corresponding barriers over the stepped surface. All energies are zero-point corrected. Atom color codes: Pd (blue), S (yellow), O (red), C (grey) and H (white).

Analysis on the reaction kinetics over RS-decorated Pd_{55}

The relevance of the calculated reaction landscape is explored by performing a microkinetic analysis of the reaction over Pd_{55}. The kinetic parameters are listed in Table S3. The (100) and (111) facets are according to the thermodynamic analysis covered by hydrogen atoms and

RS*O_2 ligands under reaction conditions. The simulations are performed in the temperature range from 275 K to 315 K, which is within the experimental regime.[7] As H_2O_2 is formed in the liquid phase during the experiments, the experimental heats of vaporization for liquid H_2O and H_2O_2 are used to account for the fact that H_2O and H_2O_2 desorb to the liquid phase (see details in Supporting Information).

Readsorption of H_2O is important as the desorption step is endothermic and will effectively hinder O_2 adsorption on the edge sites. The effect of site blocking could be accounted for by scaling the number of available site according to a Boltzmann distribution, however, we have chosen not to scale the number of available sites, which means that the calculated turnover frequency (TOF) is overestimated.

Figure 5 shows the TOF of the formation of H_2O_2 and H_2O over the RS-decorated nanoparticle as a function of temperature. We find that the TOF for H_2O_2 formation has a weak temperature dependence, whereas the TOF for H_2O formation increases with temperature. The TOF for H_2O surpasses that of H_2O_2 formation at 292 K.

The selectivity towards H_2O_2 formation decreases with increasing temperature; from 0.62 at 275 K to 0.33 at 315 K (Figure 5). Freitas et al.[14] measured direct formation of H_2O_2 over hexanethiolate-decorated Pd nanoparticle and recorded a selectivity of 0.56 towards H_2O_2 at 273 K. The simulated selectivity is in good agreement with the experimental value. As the selectivity towards H_2O_2 formation decreases with increasing temperature, direct H_2O_2 formation over the thiolate-decorated Pd nanoparticle should be performed at low temperatures.

A degree of rate control (DRC) analysis (Figure S9) shows that the first hydrogenation step from O*O to O*OH has a DRC close to one over the entire temperature interval. The second hydrogenation step to H_2O_2 has a DRC that increases from 0.2 to 0.5. The DRC of the second hydrogenation step is balanced by a negative DRC for the O*OH decomposition to O* and O*H. The sum of all DRCs is one for all temperatures. The O*OH formation step dominates the reaction rate, which implies that the availability of O*O species is limited. Similar with the concept of DRC, a degree of selectivity control (DSC) analysis is performed (see Figure S10). The second hydrogenation step to form H_2O_2 has a DSC that increases from 0.35 to 0.65 over the temperature interval, which is balanced by a negative DSC for the decomposition of O*OH.

The reaction orders in H_2 and O_2 were recently measured for bare Pd particles.[22] The reaction order for H_2O_2 formation over PdH in water solution was measured to be close to zero for H_2, whereas it was measured to be positive for O_2. Using the same reaction conditions (the H_2 pressure is ramped from 100 to 1000 kPa with an O_2 pressure of 60 kPa, and the O_2 pressure is ramped from 10 to 100 kPa with a H_2 pressure of 60 kPa), we find that the reaction order in H_2 is slightly positive, whereas it is clearly positive in O_2 for both bare and RS-decorated Pd (see Figure S11), which is in agreement with Ref. [22] The positive reaction order in O_2 is consistent with the high DRC for O*O hydrogenation.

To experimentally verify the enhanced selectivity towards H_2O_2 formation by thiolate- decoration over Pd catalysts, the concentration of H_2O_2 from the direct synthesis is measured (Figure 6) in a batch reactor at similar measured values of H_2 conversions (Figure S14). At a given condition, the concentration of H_2O_2 is clearly increased over the ethanethiolate-decorated Pd compared with the bare Pd. The yield of H_2O_2 from the thiolate-decorated Pd catalyst is much higher than the yield from the bare Pd catalyst, which indicates the selectivity towards the formation of H_2O_2 is dramatically enhanced by the ligand-decoration over Pd. The results obtained in Figure 6 were measured under O_2-excess condition (1–3 % H_2 and 8.4 % O_2), but similar large enhancements in H_2O_2 yield were obtained under H_2 excess; for example, under 3.0 % H_2 and 2.1 % O_2, and similar conversion values, an H_2O_2 yield of 9.4 ± 0.16 mmol was obtained for the ethanethiolate-decorated catalyst, while the undecorated catalyst produced only 0.7 ± 0.04 mmol.

We also measured the effect of H_2 pressure on the H_2O_2 yield (Figure 6). Increasing the H_2 pressure led to a higher accumulation of the product H_2O_2 at similar values of
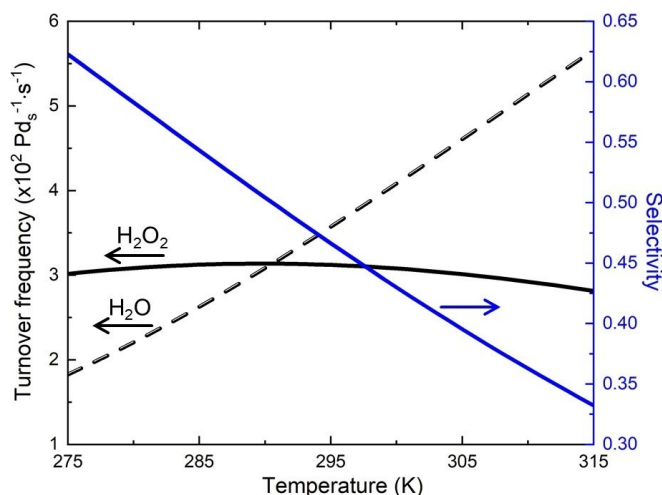

Figure 5. Simulated turnover frequency for H_2O_2 and H_2O formation on the RS-decorated Pd_{55} cuboctahedron as a function of temperature. The selectivity towards formation of H_2O_2 is given in blue. Reactant pressures: $P(H_2) = P(O_2) = 60$ kPa.
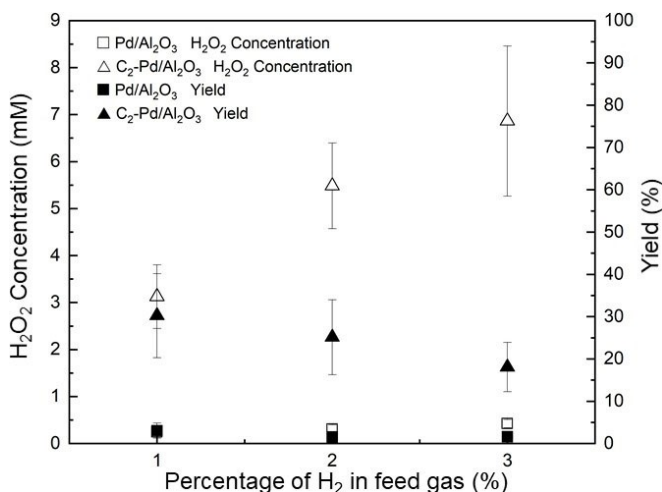

Figure 6. Measured data for direct H_2O_2 synthesis at 295 K on bare Pd and C_2H_5S-decorated (C_2-) Pd in a batch reactor using 67 % methanol in deionised water as the solvent with three different H_2 concentrations in the feed gas. The total pressure is 1380 kPa and O_2 concentration is kept at 8.4 %.

conversion (Figure S14), consistent with a positive order in H_2 for the direct synthesis reaction predicted from the model. However, the fractional yield of H_2O_2 was decreased, suggesting that the formation of water from the series reaction of H_2O_2 becomes a significant issue at high H_2 pressures and high conversions.

Discussion

Ligand-functionalization of Pd has shown to enhance the selectivity in direct H_2O_2 formation from H_2 and O_2.[10,14] Our first-principles based kinetic study show that the ligands can promote the reaction in two different ways; one is to improve the H_2O_2 selectivity owing to suppression of non-selective reactions, and the other is to improve the reaction by promoting the pathway for H_2O_2 formation.

Site blocking. One important effect of the ligands is to prevent the unwanted scission of the O–O bond by increasing the decomposition barriers of the intermediate species (O*O and O*OH). The thiolate ligands occupy hollow sites, which are the preferred sites for atomic oxygen. The site blocking effect of RS is similar to the effect of adsorbed hydrogen, which reduces the probability of O–O bond breaking.[15] However, whereas the local coverage of hydrogen can vary based on the reaction conditions, the strong RS–Pd bond should make the site-blocking from thiolates more efficient than that of hydrogen. The decomposition barrier O*OH over the RS-decorated PdH(335) [1.62 eV] is higher than the corresponding barrier over non-decorated PdH(211) surface (0.34 eV).[15]

Modification of the Pd electronic structure. Reactivity properties of transition metal surfaces are known to scale with the d-band center.[31] The d-band center for a Pd atom at the edge of Pd(335) is calculated to be -1.60 and -2.07 eV for the bare and RS-decorated case, respectively (see Figure S7). Thus, the RS-ligands clearly modify the electronic structure of the adsorption sites. The d-band center is shifted even further for the Pd-hydride. The d-band center is -2.09 eV and -2.53 eV for the non-decorated and RS-decorated β-phase Pd-hydride, respectively. The shift in d-band center correlates with the change in the O_2 adsorption energy. The adsorption energy of O_2 is -1.38 eV for bare Pd(335), -0.47 eV for RS-decorated Pd(335), -0.36 eV for PdH(335), and -0.29 for RS-decorated PdH-(335). Thus, one clear effect from the ligands is that they dramatically lower the binding affinity of O-containing species (e.g. O_2 and O) on the surface. As a high oxygen adsorption energy correlates with facile O–O bond rupture, the significant RS-induced modification of the surface electronic structure promotes high selectivity.

Ligand mediated proton transfer. The facile proton transfer via the oxidized thiolate RS*O_2-ligands to O*OH species forming HO*OH brings new insights to the reaction mechanism. The formation of HO*OH from O*OH and H* is associated with a barrier of 0.71 eV, whereas the ligand-mediated transfer is 0.41 eV. Notably, without the ligand mediated H- transfer mechanism, the formation rates of H_2O_2 would be considerably lower (Figure S13). That is, while site blocking and electronic RS-induced modification of the Pd electronic structure can lead to suppression of undesired reaction pathways, it is only when combined with facile proton transfer that significant yields are obtained. We note that another indirect proton transfer mechanism has been suggested where H_2O_2 is formed via sequential protonation of adsorbed O_2 and OOH from H^+ in the solution.[12,22] Moreover, DFT calculations indicate that the formation of hydronium from adsorbed H on a Pd-surface is associated with low barriers.[15] The finding of a ligand mediated H-transfer mechanism constitutes an additional path for efficient hydrogen transfer, which does not depend on the orientation of the water molecules in the solution. The slow relaxation of H_2O close to a reacted surface reduces the prefactor in the rate constant.[32] The facile H-transfer via RS*O_2-ligands implies that ligands can be used to maintain a three-dimensional environment over the Pd sites that allows for efficient hydrogen transfer. This is an important aspect that presumably is common for many different types of ligands.

Conclusion

We have explored the reaction mechanism for direct formation of H_2O_2 from H_2 and O_2 over methylthiolate-decorated Pd(335) and Pd_{55} by combining density functional theory based mean-field kinetic modeling and experiments. The coverage of the thiolate ligands is determined by a thermodynamic analysis. It is shown that the coverage of the RS-ligands during reaction conditions is ≈ 0.4 on Pd(335) and 0.6 on Pd_{55}. We find that the RS-ligand is oxidized to RSO_2, which constitutes the effective ligand.

The potential energy landscape for direct formation of H_2O_2 over Pd(335) and Pd_{55} and the kinetic analysis uncover multiple roles of the RSO_2 ligands. The ligands i) block hollow sites, which hinders O–O bond breaking, ii) modifies the electronic structure of Pd in a way that the adsorption energy of O_2 is reduced, iii) solvates intermediates and products, which facilitates the forward reaction, and iv) provides an efficient ligand-mediated H-transfer mechanism.

The atomistic understanding provided by our combined DFT and kinetic modeling approach gives handles to further enhance the activity and selectivity for direct H_2O_2 formation over Pd nanoparticles, for example by ligand design to modify the O_2 adsorption energy, provide efficient solvation and further enhance the ligand-mediated hydrogen transfer steps.

Acknowledgements

[1] J. Edwards, B. Solsona, E. Ntainjua, A. Carley, A. Herzing, C. Kiely, G. Hutchings, *Science* **2009**, *323*, 1037–1041.

[2] "Hydrogen Peroxide Market Size, Share & Trends Analysis Report By Function (Oxidant, Disinfectant, Bleaching), By Application (Healthcare, Wastewater Treatment), By Region, and Segment Forecasts, **2020–2027**" can be found at https://www.grandviewresearch.com/.

[3] R. Noyori, M. Aoki, K. Sato, *Chem. Commun.* **2003**, 1977–1986.

[4] G. Goor, J. Glenneberg, S. Jacobi, *Ullmann's Encycl. Ind. Chem., Vol. 18*, Wiley-VCH, Weinheim, **2012**, pp. 393–427.

[5] S. Siahrostami, A. Verdaguer-Casadevall, M. Karamad, D. Deiana, P. Malacrida, B. Wickman, M. Escudero-Escribano, E. A. Paoli, R. Frydendal, T. W. Hansen, et al., *Nat. Mater.* **2013**, *12*, 1137–1143.

[6] J. Campos-Martin, G. Blanco-Brieva, J. Fierro, *Angew. Chem. Int. Ed.* **2006**, *45*, 6962–6984; *Angew. Chem.* **2006**, *118*, 7116–7139.

[7] D. Flaherty, *ACS Catal.* **2018**, *8*, 1520–1527.

[8] Q. S. Liu, J. C. Bauer, R. E. Schaak, J. H. Lunsford, *Appl. Catal. A* **2008**, *339*, 130–136.

[9] Y. Han, Z. Zhong, K. Ramesh, F. Chen, L. Chen, T. White, Q. Tay, S. Yaakub, Z. Wang, *J. Phys. Chem. C* **2007**, *111*, 8410–8413.

[10] G. M. Lari, B. Puértolas, M. Shahrokhi, N. López, J. Pérez-Ramírez, *Angew. Chem. Int. Ed.* **2017**, *56*, 1775–1779; *Angew. Chem.* **2017**, *129*, 1801–1805.

[11] C. Samanta, *Appl. Catal. A* **2008**, *350*, 133–149.

[12] N. Wilson, D. Flaherty, *J. Am. Chem. Soc.* **2016**, *138*, 574–586.

[13] J. Edwards, G. Hutchings, *Angew. Chem. Int. Ed.* **2008**, *47*, 9192–9198; *Angew. Chem.* **2008**, *120*, 9332–9338.

[14] L. F. de L. e Freitas, B. Puértolas, J. Zhang, B. Wang, A. S. Hoffman, S. R. Bare, J. Pérez-Ramírez, J. W. Medlin, E. Nikolla, *ACS Catal.* **2020**, *10*, 5202–5207.

[15] L. Chen, J. W. Medlin, H. Grönbeck, *ACS Catal.* **2021**, *11*, 2735–2745.

[16] J. S. Jirkovský, I. Panas, E. Ahlberg, M. Halasa, S. Romani, D. J. Schiffrin, *J. Am. Chem. Soc.* **2011**, *133*, 19432–19441.

[17] T. Ricciardulli, S. Gorthy, J. S. Adams, C. Thompson, A. M. Karim, M. Neurock, D. W. Flaherty, *J. Am. Chem. Soc.* **2021**, *143*, 5445–5464.

[18] T.-T. Huynh, W.-H. Huang, M.-C. Tsai, M. Nugraha, S.-C. Haw, J.-F. Lee, W.-. N. Su, B. J. Hwang, *ACS Catal.* **2021**, *11*, 8407–8416.

[19] S. J. Freakley, Q. He, J. H. Harrhy, L. Lu, D. A. Crole, D. J. Morgan, E. N. Ntain- jua, J. K. Edwards, A. F. Carley, A. Y. Borisevich, et al., *Science* **2016**, *351*, 965–968.

[20] J. Li, K. Yoshizawa, *Catal. Today* **2015**, *248*, 142–148.

[21] Q. Liu, J. Lunsford, *Appl. Catal. A* **2006**, *314*, 94–100.

[22] J. S. Adams, A. Chemburkar, P. Priyadarshini, T. Ricciardulli, Y. Lu, V. Maliekkal, A. Sampath, S. Winikoff, A. M. Karim, M. Neurock, M. Neurock, D. Flaherty, *Science* **2021**, *371*, 626–632.

[23] C. A. Schoenbaum, D. K. Schwartz, J. W. Medlin, *Acc. Chem. Res.* **2014**, *47*, 1438–1445.

[24] E. M. Dietze, L. Chen, H. Grönbeck, *J. Chem. Phys.* **2022**, *156*, 064701.

[25] C.-H. Lien, J. W. Medlin, *J. Catal.* **2016**, *339*, 38–46.

[26] G. Kumar, C.-H. Lien, M. J. Janik, J. W. Medlin, *ACS Catal.* **2016**, *6*, 5086–5094.

[27] J. C. Love, D. B. Wolfe, R. Haasch, M. L. Chabinyc, K. E. Paul, G. M. Whitesides, R. G. Nuzzo, *J. Am. Chem. Soc.* **2003**, *125*, 2597–2609.

[28] M. Moreno, F. J. Ibanez, J. B. Jasinski, F. P. Zamborini, *J. Am. Chem. Soc.* **2011**, *133*, 4389–4397.

[29] P. E. Laibinis, G. M. Whitesides, D. L. Allara, Y. T. Tao, A. N. Parikh, R. G. Nuzzo, *J. Am. Chem. Soc.* **1991**, *113*, 7152–7167.

[30] K. R. Kahsar, D. K. Schwartz, J. W. Medlin, *J. Mol. Catal. A* **2015**, *396*, 188–195.

[31] B. Hammer, *Top. Catal.* **2006**, *37*, 3–16.

[32] D. T. Limmer, A. P. Willard, P. Madden, D. Chandler, *Proc. Natl. Acad. Sci. USA* **2013**, *110*, 4200–4205.